Wasted thermal energy recovery in heavy duty diesel vehicles using a thermoelectric/heat exchanger device

Olívia C. Rosa[a], Amir A. M. Oliveira[b] and Roberson A. Oliveira[c]

[a] Federal University of Santa Catarina, Florianópolis, Brazil, oliviacrosa@gmail.com ***(CA)***
[b] Federal University of Santa Catarina Florianópolis, Brazil, amir.oliveira@gmail.com,
[c] Volvo do Brasil Veículos Ltda., Curitiba, Brazil, roberson.oliveira@volvo.com

Abstract:
This study aims at investigating the use of a thermoelectric/heat exchanger device coupled to the exhaust pipe to increase energy efficiency in heavy-duty diesel vehicles during cold-start. The performance of the thermoelectric/heat exchanger device is evaluated by simulation both in steady state and in transient regimes. The engine gas exchange was modelled as a one-dimensional compressible flow and cylinder heat loss was taken into account using average convection and radiation exchange coefficients. A Bi_2Te_3 thermoelectric system was modelled as a series of thermoelectric cells coupled to a counter-flow heat exchanger adapted to the exhaust pipe. The results indicate that optimum engine performance of 53.5 kW occurs at 1600 rpm and peak cylinder pressure and temperature at these conditions are 13.5 MPa and 1770 K. For this operating condition, 8 kJ/cycle is lost to exhaust. The amount of energy recovered is estimated based on fixed allowed exhaust pressure loss. Results indicate that the thermoelectric/heat exchanger device can generate 124 W of electrical power at 23 % thermal efficiency suggesting a potential for application in heavy-duty engines.
Keywords:

Heat Transfer, Diesel Engine, Heat Exchanger, Seebeck Effect, Thermoelectric Converter.

1. Introduction

Approximately 30 % of the fuel energy is lost to the exhaust flow in diesel engines. When added to the losses of the engine cooling system, they represent the largest opportunities for energy recovery in vehicles. However, this energy has relatively low thermodynamic availability and attempts to recover it usually affect negatively the engine performance through the increase in exhaust back pressure and lack of control of cylinder temperature. Also, additional equipment increase vehicle mass, again reducing the overall vehicle efficiency. Therefore, the economical recovery of engine thermal energy continues to be a challenge and several systems have been proposed, such as the thermoelectric generators (TEG).

Thermoelectric generators (TEG) directly convert thermal energy flow along a temperature difference into electrical energy. TEGs are based on the Seebeck effect, which is the electrostatic potential difference created by a temperature difference. Usually, the use of a TEG for energy recovery is hardly economically viable due to their small figure of merit, Z, a material constant of the thermoelectric pair related to the efficiency of conversion from thermal energy to electrical power. Usually, the figure of merit is rendered dimensionless when expressed as ZT, where T is the absolute temperature. Commercial materials present values of ZT around 1. Although there is no upper limit for ZT, the most advanced thermoelectric pairs present ZT of the order of 2, which provides energy conversion efficiency of about 15 % [1,2]. Due to the relative small efficiency, the use of TEG coupled to the engine exhaust pipe requires large under floor space for placing the system and increases vehicle mass, which decreases the overall energy efficiency. Also, the design of an exhaust pipe heat exchanger to recover thermal energy involves a trade-off between the thermal exchange efficiency and the exhaust gas back pressure, which also reduces the engine efficiency [3]. Therefore, the main challenge is to keep the vehicle mass and the engine back-pressure low while still recovering the most energy possible, which is an opportunity for a system optimization.

This trade-off tends to be more favourable in heavy vehicles, especially when using new high figure of merit materials. Recently, Zhao et al. [4] investigated the conductivity and high figure of merit of SnSe crystals, which are known to reach values as high as 2.6 at 923 K. Even though their industrial production still remains a challenge, the design and optimization of thermoelectric modules and heat exchangers, as well as their integration with the vehicle may provide the overall efficiency that will turn these devices viable for vehicle applications. Furthermore, the combinations of TEG with an ORC (Organic Rankine Cycle), by using a heat exchanger coupled to the exhaust pipe, could provide even higher efficiency gains.

Different materials for TEG systems have been evaluated mostly by simulation. Park and Kaviany [5] analysed and simulated a combustion thermoelectric tube using high temperature alloys. They predicted a conversion efficiency of 11.3 % for $Si_{0.7}Ge_{0.3}$ and 25 % for Bi_2Te_3 TEG pairs. Furthermore, Crane and Jackson [6] modelled and tested a TEG waste heat recovery with air cooling in a cross flow heat exchanger. The results indicated net power densities (based on heat exchanger volume) above 45 W/m^3 using Bi_2Te_3 pairs. The study showed the importance of different design variables for waste heat recovery and indicated the need to assess the manufacturing process for integrating the TEG into the heat exchanger. Karri et al. [7] simulated TEG cells placed in the exhaust stream of a sport utility vehicle (SUV) and a stationary, compressed-natural-gas-fuelled engine generator. For SUV, the results suggested a 2 to 2.3 % fuel savings using Quantum-Well material based TEG, being able to generate 100 to 400 W. However, the fuel savings decreased by about 30 %, due to rolling parasitic losses. They conclude that, under both applications, a significant fraction of the exhaust energy was rejected to the coolant.

Besides the simulations, TEG systems have also been applied to commercial engines. Hsu et al. [8] simulated and tested a system composed of 24 unit TEGs coupled to the exhaust pipe of an a Chrysler Neon (2000 cm^3 engine) obtaining 12.4 W of maximum power output at average temperature difference of 30 K. Although the efficiency was low (about 0.3 %), they considered the waste heat as a low-cost resource, therefore, the low conversion efficiency was not considered a serious issue. Yu and Chau [9] proposed a practical automotive exhaust waste heat energy recovery system using a TEG. The measurements indicated that power production in the vehicle can be up to 22.6 % when an appropriate control technique is used. Zhang et al. [10] proposed and tested a thermoelectric-photovoltaic hybrid energy system for automobiles. The power improvement ranged from 7.5 % to 9.4 % for different TEG temperature while the photovoltaic generator (PVG) irradiance was kept at its maximum. Conversely, the power improvement ranged from 4.8% to 17.9 % for different PVG irradiance while keeping the TEG temperature at its value of maximum power.

From the review above, we notice that the literature reports values of energy efficiency improvements from 2 % up to 25 %, depending on the system design and thermoelectric pair used. There is no information on the application in a heavy-duty vehicle, for which weight and back pressure constraints are not as stringent, as well as, there is no evaluation of the effect of transient phenomena. Therefore, the aim of this study is to explore the potential for energy recovery using a thermoelectric converter coupled to an exhaust pipe compact heat exchanger in heavy-duty diesel vehicles. In order to evaluate the gain in energy efficiency, the performance of the heat exchanger-thermoelectric device is evaluated by numerical simulation both in steady state and in transient regimes using the EES© software

2. Analysis

2.1. Diesel Engine

The engine modelled is a heavy-duty, high efficiency diesel engine. Each cylinder contains one intake and one exhaust valve. The cylinder is lined with a ceramic layer to provide thermal insulation of the combustion chamber. Here, only one cylinder is modelled. Figure 1 presents a rendering of the basic engine dimensions and Table 1 provides engine data. The operational characteristics of the engine, other characteristic dimensions and thermal properties used here are provided elsewhere [11], [12] and [13].

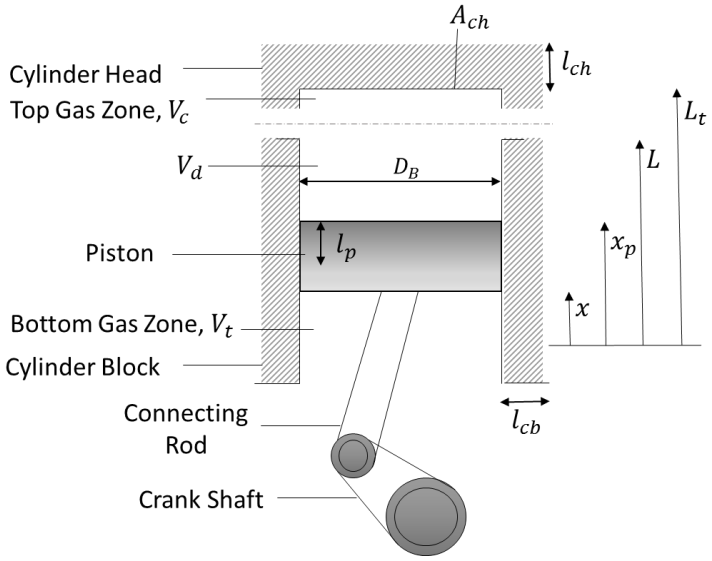

Fig. 1. The geometric parameters and variables of the diesel engine (adapted from [12]).

Table 1. Overall characteristics of the diesel engine modelled.

Parameter	Symbol, unit	Magnitude
Bore	D_B, m	0.125
Stroke	L, m	0.14
Compression Ratio	r_c	16.5
Rod length/ Crank length ratio	l / R_c	6
Skin depth of the ceramic cylinder head	l_{ch}, mm	0.4
Skin depth of the ceramic cylinder block	l_{cb}, mm	3.0
Skin depth of the piston	l_p, mm	6.0
Fuel heat of reaction with air	$\Delta h_{r,F}$, J/kg	42.5E6
Air/Fuel mass ratio	$(A/F)_a$,	30

The engine analysis aims at determining the exhaust gas temperature and mass flow as a functions of time (crank angle) for different conditions. The gas exchange was modelled as a one-dimensional, compressible flow and the gas mixture is assumed an ideal gas with constant properties. The model divides the surface layer of the aluminium cylinder head, cast iron cylinder block and aluminium piston into small control volumes to capture surface temperature variations. The remainder of the cylinder head, block and piston are divided in larger volumes.

The energy conservation equation is applied to each control volume and takes the form

$$Q_{u,\mathrm{int}} + Q_{u,exh} + Q_{u,inj} + \left\langle Q_{ku,ch} \right\rangle_{Db} + \left\langle Q_{ku,cb} \right\rangle_{Db} \left\langle Q_{ku,p} \right\rangle_{Db} = -M_f c_{p,f} \frac{dT_f}{dt} + \dot{S}_f , \qquad (1)$$

where $Q_{u,\mathrm{int}}$ is the enthalpy flow of the intake air, $Q_{u,exh}$ is the enthalpy flow of the exhaust gas, $Q_{u,inj}$ is the enthalpy flow of the fuel injection. $\left\langle Q_{ku,-ch-cb-p} \right\rangle_{Db}$ are the surface-convection heat transfer between the gas and the cylinder head, cylinder block, and piston surfaces. The energy conversion in the gas, $\dot{S}_f$, has contributions of combustion ($\dot{S}_{r,F}$), expansion cooling/compression

heating ($\dot{S}_{m,p}$), fuel evaporation ($\dot{S}_{F,Ig}$) and volumetric emission and absorption of radiation ($\dot{S}_{e,\varepsilon,-ch-cb-p} + \dot{S}_{e,\alpha,-ch-cb-p}$), i.e.,

$$\dot{S}_f = \dot{S}_{r,F} + \dot{S}_{m,p} + \dot{S}_{F,Ig} + \dot{S}_{e,\varepsilon,ch} + \dot{S}_{e,\alpha,ch} + \dot{S}_{e,\varepsilon,cb} + \dot{S}_{e,\alpha,cb} + \dot{S}_{e,\varepsilon,p} + \dot{S}_{e,\alpha,p}. \tag{2}$$

The engine heat loss was taken into account using average convection and radiation exchange coefficients. The prescribed temperature of the cooling water (380 K) was used for the analysis of the conduction through the cylinder walls and piston.

The performance parameters calculated here are the indicated power and the fuel conversion efficiency defined respectively as

$$P_{c,i} = \frac{W_{c,i,n} N}{2(rot/cycle) \times 60(s/\min)}, \tag{3}$$

$$\eta_F = \frac{1/\Delta h_{isfc}^{-1}}{\Delta h_{r,F}}, \tag{4}$$

where $P_{c,i}$ is the indicated power per cycle and η_F is the fuel conversion efficiency.

Each term in equations (1) and (2) are modelled as follows. The enthalpy flow of the intake air and exhaust gas are

$$Q_{u,\text{int}} = \begin{cases} \dot{M}_{a,\text{int}} c_{p,a} (T_f - T_n), & for \quad \dot{M}_{a,\text{int}} > 0 \\ 0, & for \quad \dot{M}_{a,\text{int}} \le 0 \end{cases}, \tag{5}$$

$$Q_{u,,exh} = \begin{cases} \dot{M}_{f,exh} c_{p,f} (T_f - T_e), & for \quad \dot{M}_{f,exh} < 0 \\ 0, & for \quad \dot{M}_{f,exh} \ge 0 \end{cases}. \tag{6}$$

The enthalpy flow in the fuel injected is

$$Q_{u,inj} = -\dot{M}_{F,inj} c_{p,F} (T_f - T_{F,o}). \tag{7}$$

The surface-convection heat transfer between the gas and the cylinder head, cylinder block, and piston surfaces is

$$\left\langle Q_{ku,-ch-cb-p} \right\rangle_{Db} = \frac{(T_f - T_{-ch-cb-p,o})}{\left\langle R_{ku,-ch-cb-p} \right\rangle_{D_B}}. \tag{8}$$

where the surface-convection resistance is

$$\left\langle R_{ku,-ch-cb-p} \right\rangle_{D_B} = \frac{D_B}{\langle Nu \rangle_{D_B} k_f A_{ku,-ch-cb-p}}, \tag{9}$$

where the Nusselt number is determined from the Woschni correlation [12],[13].

The energy conversion terms are

$$\dot{S}_{r,F} = \dot{M}_{r,F} \Delta h_{r,F}, \tag{10}$$

$$\dot{S}_{m,p} = V_f \frac{dp_f}{dt}, \tag{11}$$

$$\dot{S}_{F,Ig} = -\dot{M}_{F,inj}\Delta h_{ig}\,, \tag{12}$$

$$\dot{S}_{e,\varepsilon,ch} + \dot{S}_{e,\alpha,ch} = -\varepsilon_{r,f}\alpha_{r,ch}\sigma_{SB}T_{r,f}^4 A_{r,ch} + \varepsilon_{r,ch}\alpha_{r,f}\sigma_{SB}T_{ch,o}^4 A_{r,ch}\,, \tag{13}$$

where

$$\dot{S}_{e,\varepsilon,ch} + \dot{S}_{e,\alpha,ch} = +\left\langle Q_{ku,ch}\right\rangle_{D_B} - Q_{r,ch-cb} - Q_{r,ch-p} - (Q_{k,ch})_{o-1})\,. \tag{14}$$

where $Q_{r,ch-cb}$ and $Q_{r,ch-p}$ are the heat transfer by surface radiation between the cylinder head and the cylinder block and the cylinder head and piston; $(Q_{k,ch})_{o-1}$ is the heat flow rate by conduction from the cylinder surface to the interior of the cylinder head. Averaged radiative properties are modelled as in [12],[13]. The model presents crank-angle resolved exhaust pipe flow and temperature, which are imposed as thermal energy sources to the TEG modules.

2.2. Heat Exchanger

Here, we use two heat exchanger basic configurations: the concentric tube and the plate heat exchanger. The heat exchangers are shown in Fig. 2. They operate in a counter-flow arrangement and are formed by a number of individual flow modules arranged in parallel. Each flow module, by its turn, has a number of TEG modules embedded on its walls. The heat exchanger tubes are made of stainless steel AISI 304. In order to compare both configurations, the plate heat exchanger is designed with the same overall dimensions and outer and inner tube materials. Therefore, the masses are similar: 13.73 kg for concentric tubes, 14.18 kg for plate. However, due to the dimensional constraints, while the concentric tubes are formed by 25modules (D_{int}=5 cm and D_{ext}=10 cm), the plate heat exchanger has only 5 modules. ($lenght_{\text{int}}$=49 cm and $height_{\text{int}}$=5 cm).

In this study, we assume negligible heat loss to surroundings, negligible kinetic and potential energy changes, negligible fouling factors and fully developed conditions for exhaust gas and cold fluid (water) with initial conditions: T_w=297 K and $\dot{m}_w$=0.02m/s.

Fig. 2. A schematic of the concentric tube and heat exchanger with the thermoelectric junctions coupled.

For solving the heat exchanger problem, we used the effectiveness-NTU (number of transfer units) method [12], [14], [15]. The average surface-convection resistance, obtained from the thermal circuit analysis [12], is then defined as,

$$\left\langle R_u\right\rangle_L = \frac{1}{(\dot{m}c_p)_f(1-e^{-NTU})}\,. \tag{15}$$

where, as usual, $NUT = UA/(\dot{m}c_p)_{\min}$ and UA is calculated considering entrance length effects.

Finally, the energy equation for fluid nodes in the heat exchanger relates the temperature of the fluid in each section of the heat exchanger with the solid wall temperature as

$$\frac{(T_{solid,i} - T_{fluid,i})}{\langle R_u \rangle_{L,fluid}} + \left[\dot{m} c_p (T_{i+1} - T_i)\right]_{fluid} = 0, \quad (16)$$

where $T_{solid,i}$ is the wall surface temperature.

2.3. Thermoelectric Converter

Figure 3 presents a rendering of the flow (thermoelectric) tube. The temperature difference across the thermoelectric devices, placed in the heat exchanger wall separating the hot from the cold fluids, generates electric power.

Fig. 3. A schematic of the concentric tube heat exchanger's module with the TEGs.

For p- and n-type thermoelectric units, we use the properties of the commercially available bismuth telluride (Bi_2Te_3), with ZT=1.84 for T=600K and a current high-temperature material $Si_{0.7}Ge_{0.3}$, with ZT= 0.537 for T=900K. The conductors have a circular cross section $D_n = D_p = 3$ mm and have a length $L_n = L_p = 6$ mm.

The tube (module) was divided into three finite volumes as shown in Fig. 4.a. For the electrical circuit diagram, shown in Fig. (4 b), the electrical power is produced by maintaining a p-n couple junction at temperature T_h, while the electrode is at a lower temperature T_c. Furthermore there is an external load $R_{e,o}$ in the circuit. The current density Je_i in each volume is determined by setting the sum of the voltage potentials across the circuit in Fig. 4b to zero, i.e,

$$Je_i = \frac{\alpha_s (T_{solid,i} - T_{solid,j})}{R_{e,o} + R_e}, \quad (17)$$

where R_e is the combined electrical resistance of the p and n materials.

The energy equation applied for the nodes at the wall provides the temperature for the hot and cold walls in each section:

$$\frac{(T_{solid,i} - T_{fluid,i})}{\langle R_u \rangle_{L,fluid}} = \pm N_i \alpha_s Je_i T_{solid,i} + N_i \frac{R_e Je_i^2}{2} - N_i \frac{(T_{solid,i} - T_{solid,j})}{R_{k,i-j}} - \left(\rho c_p V \frac{dT}{dt}\right)_{solid,i}, \quad (18)$$

When *i* stands for the hot wall, the first term on the left-hand side is negative due to the absorption of thermal energy. The other terms are explained in [5] and [12]. The electrical power rate generated by the devices (P_e) and the electrical potential are given by

$$P_e = \sum_{i=1}^{3} N_{tubes} N_i Je_i^2 R_{e,o}, \quad (19)$$

$$\Delta\phi = \sum_{i=1}^{3} N_{tubes} N_i Je_i R_{e,o}. \quad (20)$$

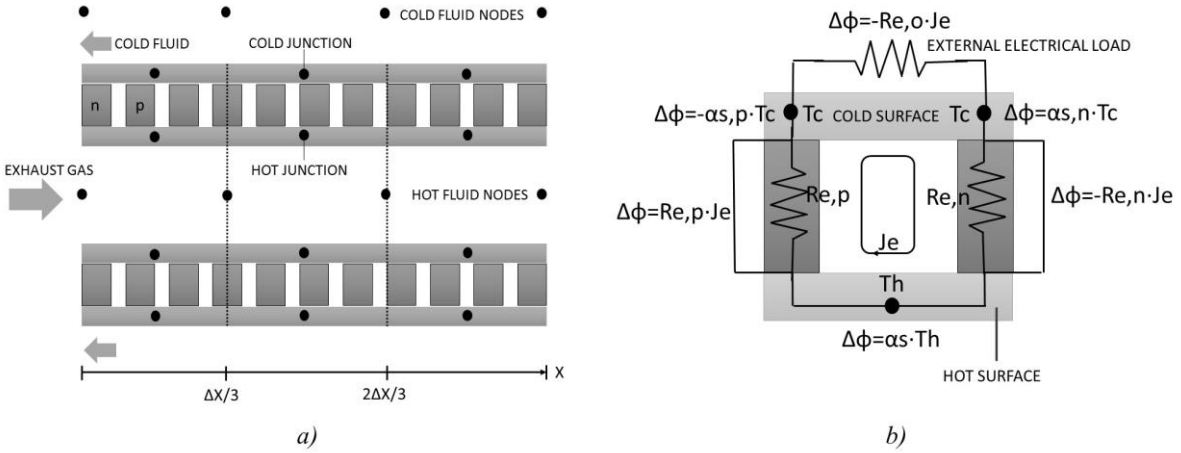

Fig. 4. a) A schematic of the thermoelectric junctions coupled to the concentric tube heat exchanger, b) Electrical circuit diagram for the thermoelectric unit.

2.4. Pressure Loss

The pressure loss (or, head loss) analysis aims at optimizing the heat exchanger design based on the hydraulic diameter and the number of modules. Losses caused by secondary flows are neglected in this analysis. Only the major losses are taken into account [16]. As a design constraint, a maximum allowable pressure loss of 2 % of the ambient pressure (abs.) was taken. Although this number can change, depending on engine design, the overall characteristics of the results remain the same.

3. Results and discussion

Figure 5a presents the indicated $p_f - V_f$ diagram covering the complete engine cycle ($\theta = 0°$ corresponds to the intake valve opening) obtained after the engine periodic steady-state regime is achieved. The net indicated work is given by the area inside the loop. In order to find an optimum operation point for the engine, we determine the performance parameters at different crank speeds. Table 2 shows the results and suggests that the best fuel efficiency of 43.6 % occurs at 1600 rpm.

Figure 5b shows the variations of the dimensionless cylinder-space volume, fluid pressure and temperature. The peak of pressure (13.5 MPa) and temperature (1770 K) occur immediately after $\theta = 360°$. Figure 6a presents the mass flow rates during intake, injection and exhaust. A small backflow ($\dot{m}_{\text{int}} < 0$) occurs during intake. The peak exhaust flow rate is taken to estimate the exhaust back pressure.

Table 2. Engine performance parameters for different crank shaft angular speeds

Engine crank shaft angular speed, rpm	Indicated power (per cylinder), kW	Fuel conversion efficiency, %	Heat lost to walls, J/cycle	Energy lost to exhaust, J/cycle
1000	33.9	43.55	496.8	8057
1600	53.5	43.62	382.2	8240
2200	69.9	41.44	338.3	7799
2800	76.5	35.64	340.5	6744
3400	90.6	34.74	358.9	6282
4000	104.0	33.93	380.5	5952

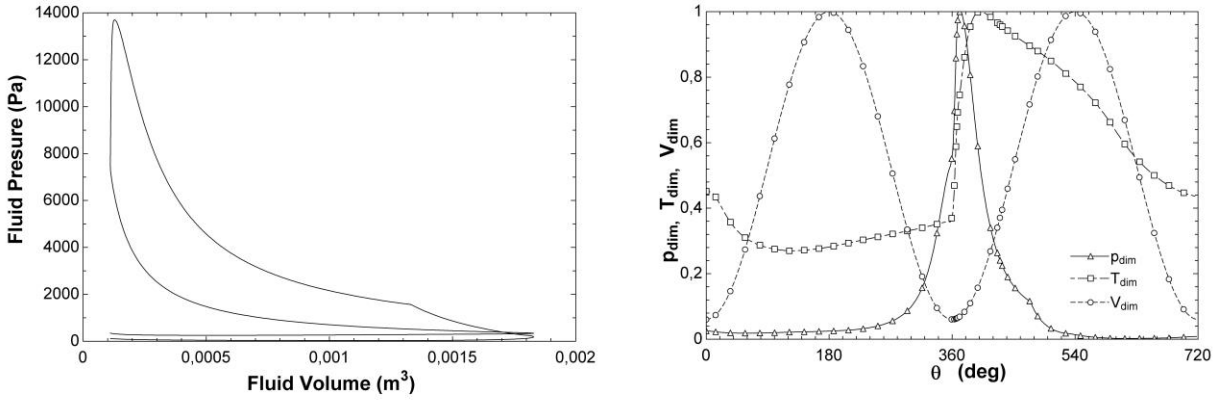

a) *b)*

Fig. 5. a) Predicted $p_f - V_f$ diagram cycle, b) Predicted dimensionless cylinder-space volume, fluid pressure and temperature for one cycle.

Figure 6b presents the number of tubes required to keep the pressure loss in the exhaust pipe constant as a function of the hydraulic diameter for different lengths of the modules. As the diameter of the pipes increase, the number of tubes required decrease. The lines represent the smaller number of pipes that must be selected for given tube diameter and length. For the results that follows, a tube diameter of 5 cm and length of 10 cm are selected, requiring 25 tubes to keep the exhaust pipe pressure loss under 2 kPa.

Assuming a fixed heat exchanger design, the transient exhaust flow can now be used to assess the transient power generated by the TEG system. Figure 7a presents the power and electrical potential as a function of elapsed time from cold-start for the two thermoelectric materials in the concentric tubes arrangement. At cold start, the temperature difference across the tube walls is maximum, resulting in a maximum power and electric potential. As the heating of the tubes proceed, steady-state is reached at about 300 s and the power and potential drop to their steady-state values. The steady-state results suggest that the electrical potential is similar, while the power for Bi_2Te_3 is 124.4 W, approximately the triple of that obtained with $Si_{0.7}Ge_{0.3}$, as suggested by the ratio of the values of their ZT.

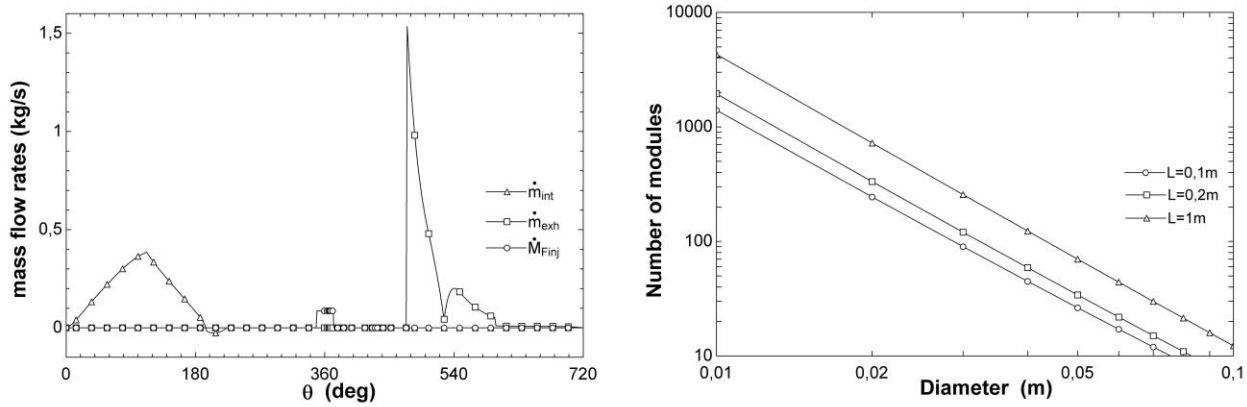

a) *b)*

Fig. 6. a) Predicted mass flow rates during intake, injection and exhaust, b) number of tubes required to keep the pressure loss in the exhaust pipe constant as a function of the hydraulic diameter for different lengths of the modules.

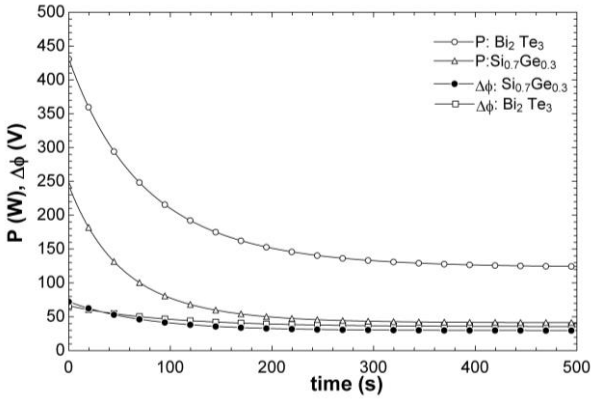

Fig. 7. Predicted generated power and electrical potential as a function of elapsed time from cold-start for two thermoelectric materials.

Based on the previously findings, the Bi_2Te_3 was used for the analysis that follows. Figure 8a shows the power generated and electrical potential for different average exhaust gas temperature. The values for steady state conditions are 81.7 W, 124.4 W and 221.4 W for temperatures of 700 K, 800 K and 1000 K, respectively. Figure 8b compares the power generated and the electrical potential for the concentric tube and the plates heat exchangers, for the same number and size of pipes. The concentric tube provides higher power and electric potential as a result of the higher current density. This occurs because the temperature difference between the cold and the hot walls is different for both designs: For the plates configuration it is 235.7 K, while for the concentric tubes it is 270.5 K. The temperature difference for the concentric tubes is higher because the average surface-convection resistance is lower, providing a higher heat transfer rate to the solid walls. On the other hand, although the steady-state power for the plates heat exchanger is lower (94.6 W), it reaches steady state faster, due to the lower thermal inertia.

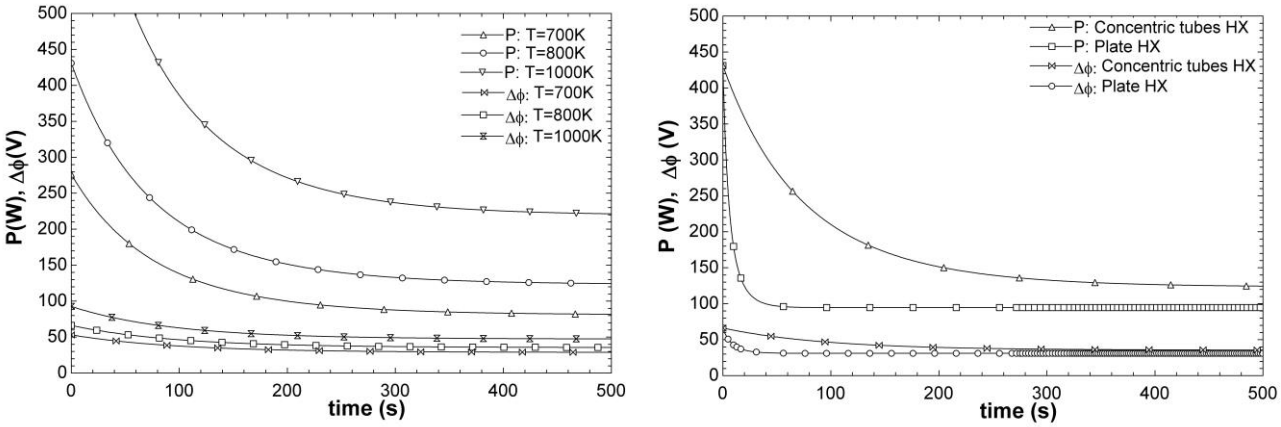

a) *b)*

Fig. 8. Predicted generated power and electrical potential as a function of elapsed time from cold-start for (a) different average exhaust gas temperature and b) different heat exchangers configurations.

Considering the energy lost to exhaust at 1600 rpm, the concentric tubes configuration, Bi_2Te_3 thermoelectric units, and exhaust temperature of 800 K, the power generated corresponds to 0.23 % of the engine power and the TEG thermal efficiency reaches 20.13 %.

4. Conclusion

Using numerical simulations, we explored the potential for energy recovery of a thermoelectric converter coupled to an exhaust pipe compact heat exchanger in diesel engines from cold-start to

steady-state. For a $Si_{0.7}Ge_{0.3}$ thermoelectric pair we found a thermal energy to electrical power conversion of at least 41 W. The TEG performance is strongly dependent of the material used, in agreement with previous results. While Bi_2Te_3 provide best results and is available commercially, the $Si_{0.7}Ge_{0.3}$ tolerates higher temperatures. The present analysis did not consider the temperature drop between the exhaust valve and the heat exchanger, being more appropriate to a close-coupled device. Additionally, for an optimum power, the external electrical load was considered equal to the combined electrical resistance of the thermoelectric conductors.

The results indicated that the power generated is maximum at cold-start and reduces in the direction of steady-state. In relation to the different configurations, the concentric tubes heat exchanger provides higher power for the same volume. However, the plate heat exchanger reaches steady state faster and requires fewer tubes to the same pressure loss. In addition, the plate heat exchanger is easier to manufacture and can possibly accommodate a larger number of thermoelectric devices. Based on best operation conditions, the concentric tubes configuration, Bi_2Te_3 thermoelectric units, 25 tubes of 5 cm diameter and 10 cm length, exhaust temperature of 800 K, pressure loss of 2 kPa, at 1600 rpm, the power generated corresponds to 0.23 % of the engine power and the TEG thermal efficiency reaches 20.13 %. These results indicates opportunities for improvements, especially during cold-start. Future work is planned to assess the loss in vehicle efficiency due to the additional mass and the modelling of the power conditioning system coupled to the TEG device.

Acknowledgments

We gratefully acknowledge the financial support by Volvo Trucks Brazil.

Nomenclature

$(A/F)_a$	air/fuel mass ratio
A	area, m^2
c_p	specific heat capacity, J/(kg·K)
D_B	bore, m
D_h	hydraulic diameter, m
e	internal surface roughness
f	friction factor
HX	heat exchanger
Je	current, A
k	thermal conductivity, W/(m·K)
L	stroke, m
l/R_c	rod length/ crank length ratio
M	mass (kg) or molar mass (kg/kmole)
N	rpm or number of nodes or number of parcels
Nu	Nusselt number
NTU	number of transferable units
p	pressure, Pa
P	power, W
Pr	Prandtl number
Q	heat flow rate, W
R	thermal resistance, K/W

r_c	compression ratio
R_g	universal gas constant 8.3145 J/(mole·K)
Re	Reynolds number
$\dot{S}$	energy conversion rate, W
T	temperature, K
u_m	velocity, m/s
W	work, J
V	volume, m^3

Greek symbols

α	absorption or Seebeck coefficient
ε	emissivity coefficient
Δh_{isfc}^{-1}	specific fuel consumption
Δh_{ig}	evaporation heat, J/(kg_fuel)
$\Delta h_{r,F}$	fuel heat of reaction with air, J/kg
Δl	nodal length, m
$\Delta\phi$	electrical potential, V
η	efficiency
μ	viscosity, (Pa·s)
ρ	density, kg/m^3
σ_{SB}	Stefan-Boltzmann constant

Subscripts and superscripts

a	air
cb	cylinder block
ch	cylinder head
e,o	external load
exh	exhaust
f	fluid
F	fuel
F,Ig	fuel ignition
inj	injection
int	intake
ku	conduction
m,p	mechanical power
n	negative thermoelectric material
p	pressure or positive thermoelectric material or piston
r	radiation
r,f	adiabatic
r,F	fuel reaction

t major loss

ll convection

w cooling water or wall

Other symbols

$\langle\ \rangle$ local spatial averaged

References

[1] Yang J., Potential applications of thermoelectric waste heat recovery in the automotive industry. International Conference on Thermoelectrics, 2005: 155 – 159.

[2] Saidur R. et al., Technologies to recover exhaust heat from internal combustion engines. Renewable and Sustainable Energy Reviews 2012: 16: 5649 – 5659.

[3] Zhao L. et al. Ultralow thermal conductivity and high thermoelectric figure of merit in SnSe crystals. Nature 2014: 508: 373 – 377.

[4] Zhang X., Chau K. T., Chan C. C., Overview of thermoelectric generation for hybrid vehicles. Journal of Asian Electric Vehicles 2008: 6(2): 1119 – 1124

[5] Park C. W., Kaviany M., Combustion- thermoelectric tube. Journal of Heat Transfer 2000: 122: 721 – 729.

[6] Crane D. T., Jackson G. S., Optimization of cross flow heat exchangers for thermoelectric waste heat recovery. Energy conversion and management 2004: 45: 1565 – 1582.

[7] Karri M. A., Thacher E. F., Helenbrook B. T., Exhaust energy conversion by thermoelectric generator: two case studies. Energy conversion and management 2011: 52: 1596 – 1611.

[8] Hsu C. T et al., Experiments and simulations on low-temperature waste heat harvesting system by thermoelectric power generators. Applied Energy 2011: 88: 1291 – 1297.

[9] Yu C., Chau K. T., Thermoelectric automotive waste heat recovery using maximum power point tracking. Energy conversion and management 2009: 50: 1506 – 1512.

[10] Zhang X., Chau K. T., Chan C. C., Gao S., An automotive thermoelectric-photovoltaic hybrid energy system. Xiaodong Zhang; Chau, K.T.; Chan, C.C.; Gao, S., An automotive thermoelectric-photovoltaic hybrid energy system. Vehicle Power and Propulsion Conference 2010: IEEE:1 – 5.

[11] Park C. W., Kaviany M., Evaporation-combustion affected by in-cylinder, reciprocating porous regenerator. Journal of Heat Transfer 2002: 124: 184 – 194.

[12] Kaviany M., Principles of heat transfer. New York, USA: John Wiley & Sons, Inc. 2002.

[13] Heywood J. B., Internal Combustion Engine Fundamentals. New York, USA: McGraw Hill, 1968. p. 304-308 and 678-682.

[14] Nellis G., Klein S., Heat transfer. New York, USA: Cambridge University Press, 2012. p. 647 -668 and p. 823 – 825.

[15] Incropera F. P., Dewitt D. P. Fundamentals of Heat and Mass Transfer. 4 ed. New York, USA: John Wiley Sons, 1996. p. 444 – 445, p. 582 – 595.

[16] Fox R. W., Mcdonald A. T., Pritchard P. J., Introduction to fluid mechanics. 6 ed. Rio de Janeiro: LTC, 2006. p 345 – 359.